ACS NANO
Cite This: ACS Nano 2017, 11, 12411−12418
www.acsnano.org

ARTICLE

Self-Powered Electrostatic Filter with Enhanced Photocatalytic Degradation of Formaldehyde Based on Built-in Triboelectric Nanogenerators

Yawei Feng,[†] Lili Ling,[†] Jinhui Nie,[‡] Kai Han,[‡] Xiangyu Chen,*[,‡] Zhenfeng Bian,*[,†] Hexing Li,*[,†] and Zhong Lin Wang*[,‡,§]

[†]Education Ministry Key and International Joint Lab of Resource Chemistry and Shanghai Key Lab of Rare Earth Functional Materials, Shanghai Normal University, Shanghai 200234, PR China

[‡]Beijing Institute of Nanoenergy and Nanosystems, Chinese Academy of Sciences, Beijing 100083, PR China

[§]School of Materials Science and Engineering, Georgia Institute of Technology, Atlanta, Georgia 30332-0245, United States

Supporting Information

ABSTRACT: Recently, atmospheric pollution caused by particulate matter or volatile organic compounds (VOCs) has become a serious issue to threaten human health. Consequently, it is highly desirable to develop an efficient purifying technique with simple structure and low cost. In this study, by combining a triboelectric nanogenerator (TENG) and a photocatalysis technique, we demonstrated a concept of a self-powered filtering method for removing pollutants from indoor atmosphere. The photocatalyst P25 or Pt/P25 was embedded on the surface of polymer-coated stainless steel wires, and such steel wires were woven into a filtering network. A strong electric field can be induced on this filtering network by TENG, while both electrostatic adsorption effect and TENG-enhanced photocatalytic effect can be achieved. Rhodamine B (RhB) steam was selected as the pollutant for demonstration. The absorbed RhB on the filter network with TENG in 1 min was almost the same amount of absorption achieved in 15 min without using TENG. Meanwhile, the degradation of RhB was increased over 50% under the drive of TENG. Furthermore, such a device was applied for the degradation of formaldehyde, where degradation efficiency was doubled under the drive of TENG. This work extended the application for the TENG in self-powered electrochemistry, design and concept of which can be possibly applied in the field of haze governance, indoor air cleaning, and photocatalytic pollution removal for environmental protection.

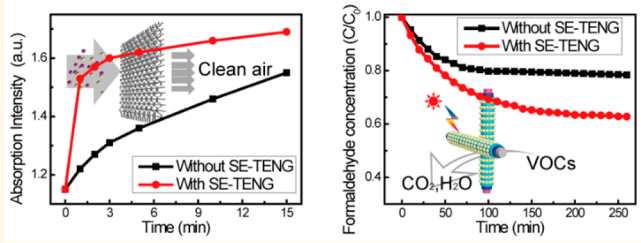

KEYWORDS: *triboelectric generator, electrostatic adsorption, photocatalysis, formaldehyde degradation, air filter*

In the past decades, atmospheric pollution caused by particulate matter (PM), gaseous pollutants, such as volatile organic compounds (VOCs) and NO_x has become a serious environmental problem to threaten human life.[1,2] For example, asthma and chronic bronchitis can be exacerbated by the effects of PM on lungs,[3] formaldehyde caused by indoor decoration can make people feel uncomfortable or even poisoned.[4] Consequently, several techniques have been employed to purify the indoor atmospheric pollution, including high efficiency particulate air (HEPA) filter, polymer nanofiber filter,[5] activated carbon absorption,[6] plant species removal, and so on.[7] However, each of these techniques still remain challenging. For example, HEPA and polymer filters are inefficient for VOC removal; activated carbon has limited absorptivity and easily creates secondary contamination; plant removal is time-consuming. Another widely used filtering technology is an electrostatic adsorption method based on a high electrostatic field, which universally collects various suspended particles with a very high efficiency.[8] However, the applied high electric field increases the consumption of energy, and the ozone generation caused by the high electric field can be a secondary pollutant to the environment. Hence, a series of studies should be continuously devoted to pursue more efficient and more convenient methods for the absorption and degradation of various atmospheric pollutants.

Since the invention of triboelectric nanogenerators (TENGs), they have been employed as the energy harvesting

Received: September 11, 2017
Accepted: November 1, 2017
Published: November 30, 2017

DOI: 10.1021/acsnano.7b06451
ACS Nano 2017, 11, 12411−12418

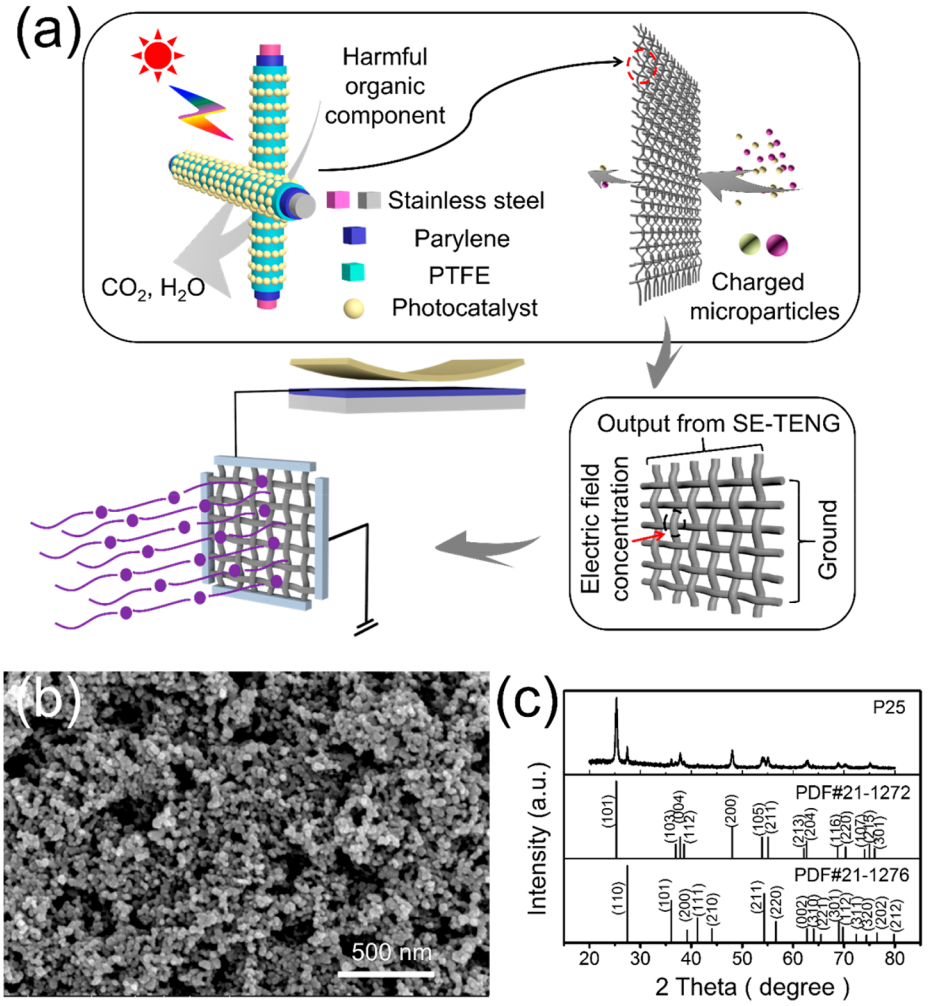

Figure 1. (a) The proposed schematic images for self-powered absorption from electrostatic Coulomb force based on triboelectrification effect and self-cleaning based on photocatalytic effect. (b) SEM image and (c) XRD pattern of the used photocatalyst commercial P25 nanoparticles.

element for various nano- and microsystems.[9−11] By converting various mechanical vibrations available in our living environment into electrical energy, TENGs can be directly used to charge batteries, light LEDs, or drive many electromechanical devices.[12−19] Moreover, based on the effect of electrostatic absorption from the tribo-induced high electrostatic field, TENGs can also be used as a filter device to remove pollutant particles (PM 2.5) in the air. In comparison with conventional electrostatic precipitation by applying high voltages, the TENG-based filter device shows several advantages, such as high efficiency, no energy consumption, and no ozone generation.[20−22] However, the self-powered absorption can only collect PM, and it offers no chemical degradation of the pollutants, which is not enough for indoor air purification. On the other hand, photocatalysis is a powerful technology for solving environmental problems, including degradation of aqueous and gaseous pollutants.[23−25] The photocatalyst materials can be smoothly integrated into the design of TENG devices because the materials used for fabricating TENG are rather diverse. Thus, the integration of TENG technique and photocatalysis technology will develop an improved self-powered filtering method, that is able to effectively remove and degrade the VOCs, especially formaldehyde, for the indoor atmosphere.

Here, we demonstrate a self-powered filter by combining TENG and photocatalysis technique for removing organic vapor pollutants in the indoor atmosphere. The filtering network is fabricated by weaving a series of polymer-coated steel wires, while the photocatalyst P25 or Pt/P25 is embedded on the surface of polymer-coated stainless steel wires. A high electric field can be induced by using the filtering network as the output terminal of single electrode triboelectric nanogenerator (SE-TENG). Moreover, the high electrostatic field generated by TENG can induce electrostatic adsorption effect, collecting tiny particles in the air, which can also enhance the photocatalytic effect for degrading the pollutants in the indoor air. Both electrostatic adsorption and TENG-enhanced photocatalytic effect can be achieved by this filtering device. This work shows the potential of TENG for indoor air cleaning and photocatalytic pollution control.

RESULTS AND DISCUSSION

The structural design of the self-powered pollutant filter based on TENG and photocatalysis techniques is shown in Figure 1. The network device was woven from PTFE-coated metal wires, which can serve as a filter for the pollutants. The polymer-coated stainless steel wires were prepared as in Figure 1a, and the detailed fabrication process is described in the Experimental Section. The raw stainless steel wire was about 100 μm in

DOI: 10.1021/acsnano.7b06451
ACS Nano 2017, 11, 12411−12418

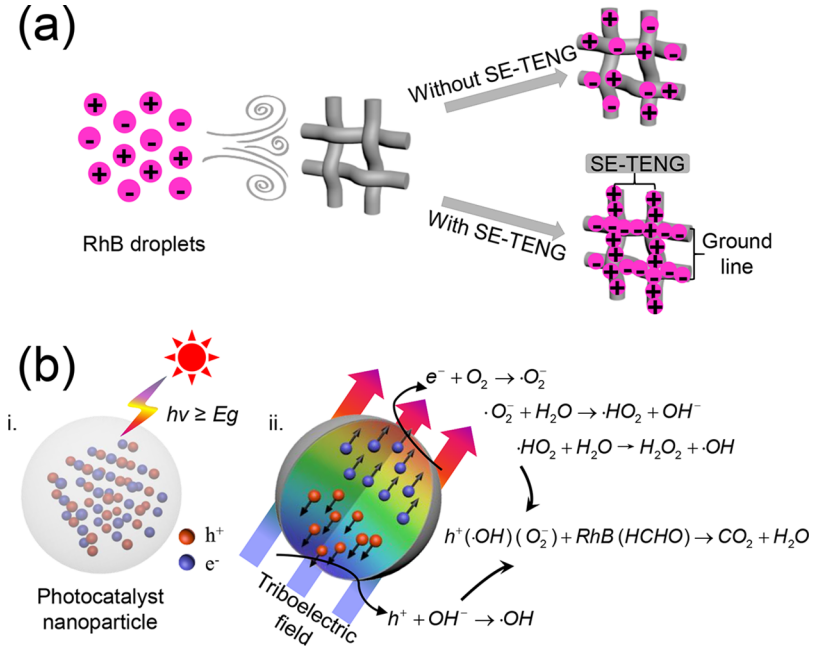

Figure 2. Detailed schematic illustration of how SE-TENG enhances (a) electrostatic absorption of RhB dye and (b) photocatalytic degradation of RhB and formaldehyde.

diameter (Figure S1a) with an internal resistance <0.1 Ω. On the surface of steel wire, 3 μm of parylene (Figure S1b) and 5 μm of PTFE (Figure S1c) were successively deposited as the dielectric layer using vacuum vapor deposition and dip-coating methods, respectively. After annealing at 300 °C, the PTFE layer shrunk due to fusion (Figure S1e). To realize photocatalytic VOC degradation, the photocatalyst, commercial P25 or noble metal Pt-loaded P25 (Pt/P25), was embedded on the surface of the PTFE layer through the dip-coating method in P25 or Pt/P25/PTFE suspension. The fabricated network device is shown in Figure S2. Two groups of strip electrodes (Al tape) were attached on the frame of the filter. All the metal wires in vertical or horizontal directions were electrically connected to the same strip electrodes (see the inset in Figure 1a). The metal wires in vertical and horizontal direction were separated by the dielectric layers, and the electrostatic field can be established between them. A SE-TENG was applied for the system, while the filter network was connected between the SE-TENG and the ground, as shown in Figure 1a. With the output voltage from TENG, the surface of filter network could be charged, which led to a strong electrostatic field along the wires. Consequently, the tiny dust, microparticles, or polar organic pollutant molecules could be adhered to or absorbed on the surface of the PTFE-coated network, as shown in Figure 1a. With embedded commercial P25 or Pt-loaded P25 nanoparticles (photocatalyst) on the surface layer, the filter network could realize the degradation of indoor blastomogenic gaseous matter, like formaldehyde, into nontoxic CO_2 and water under UV irradiation. The applied commercial P25 particles are nanosized (Figure 1b) and consist of anatase (PDF # 21-1272) and rutile (PDF # 21-1276) phases (Figure 1c), which possess strong photon response under UV irradiation. Meanwhile, the photocatalytic performance could also be enhanced by restraining the recombination of hole−electron pairs under the surface electrostatic field.

The detailed schematic of how SE-TENG enhances electrostatic absorption and photocatalytic pollutant degradation is shown in Figure 2. To demonstrate electrostatic absorption and enhanced photocatalytic degradation, azo dye RhB was selected as a sample pollutant. After the spraying process, RhB steam carried some electrostatic charges, resulting from friction with compressed air (see Figure 2a).[26−28] For the filter network without electric field, most RhB droplets passed through the mesh aperture and only a small amount of droplets precipitated randomly on the surface of the filter. When the filter network was excited by SE-TENG, a strong electrostatic field was generated on each wire. Thus, the charged RhB droplets can be absorbed on the filter due to Coulomb force and the absorbed dosage on the filter network increased significantly. This process is the TENG-enhanced electrostatic absorption. The typical photocatalytic degradation process is shown in Figure 2b. Photocatalyst first captures the photons with an energy larger than the band gap to generate electron−hole pairs, then the photogenerated pairs separate and migrate to the surface of the photocatalyst to induce the oxidation−reduction reaction on the surface of the catalyst. However, the severe recombination of free electrons and holes greatly restricts the photocatalytic process. In this case, the strong electric field provided by SE-TENG can help to separate the electron−hole pairs and promote the migration of the charges to the surface of photocatalyst. The separated electrons and holes can generate hydroxyl group and superoxide radical based on the reaction with water and oxygen. Ultimately, holes, as well as hydroxyl groups and superoxide radical, can directly or indirectly contribute to the degradation of the pollutants, as shown in Figure 2b.

The working principle of SE-TENG is based on the coupling effects of contact electrification and electrostatic induction, as shown in Figure S3. The contact between dielectric layer and Al electrode results in an electrification process occurring at the interface. And the successive separation motion can establish a strong electrostatic field between Al electrode and ground. In order to balance this field, the charges from the grounded position move toward the Al electrode, as can be seen in Figure

DOI: 10.1021/acsnano.7b06451
ACS Nano 2017, 11, 12411−12418

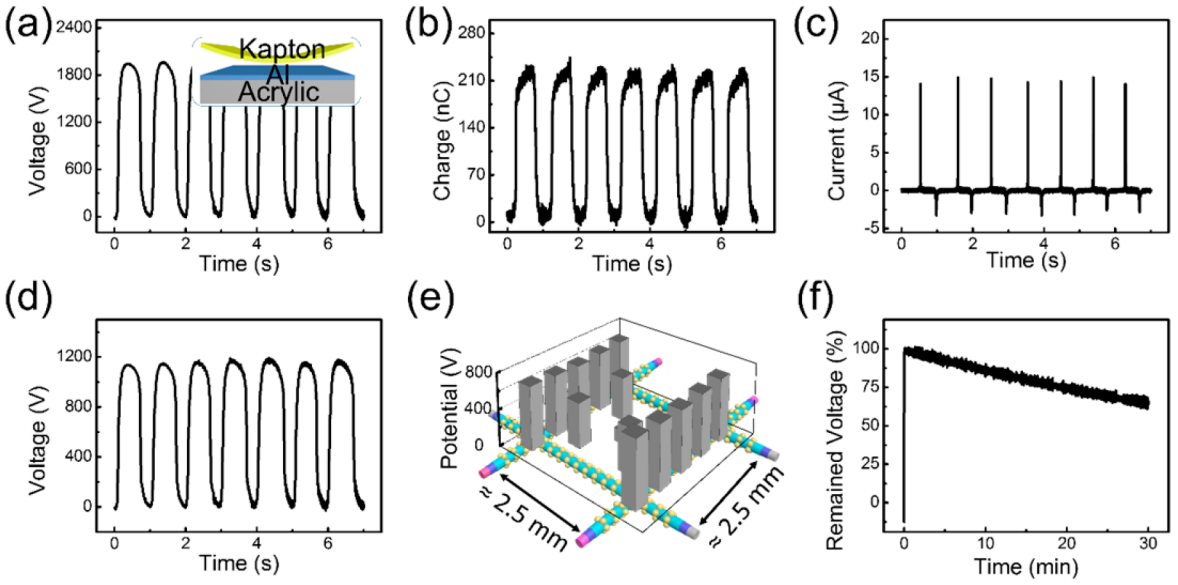

Figure 3. (a) The open-circuit voltage, (b) the maximum transferred charges, and (c) the short-circuit current of the SE-TENG. The inset of panel a is a schematic image of the fabricated SE-TENG. (d) The voltage on the filter network device fabricated by P25/PTFE/parylene-coated stainless steel when combining the SE-TENG. (e) The surface potential distribution on one aperture hole and (f) the voltage drop on the filter network within 30 min.

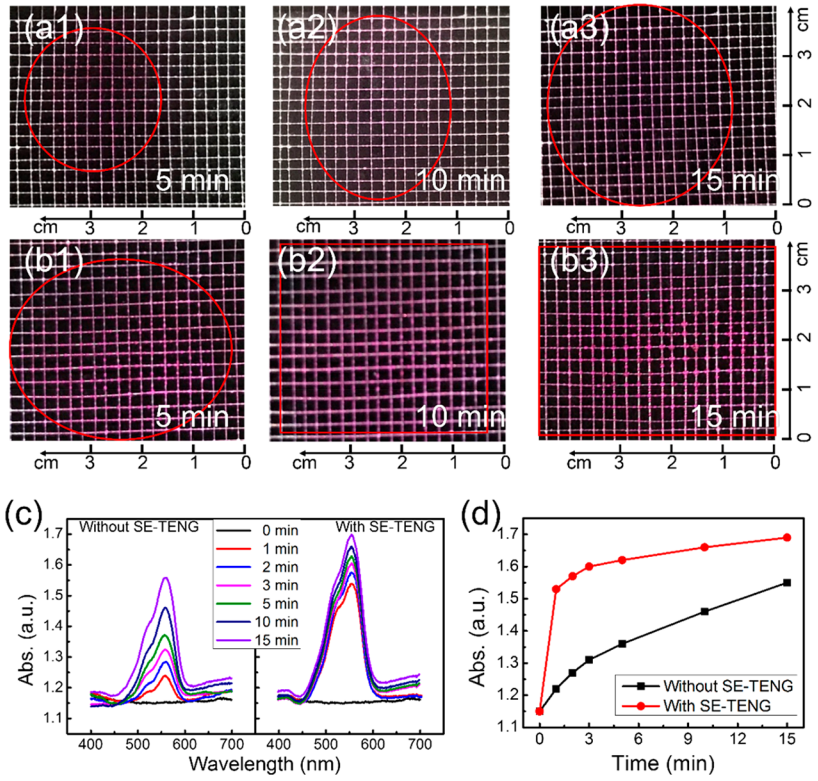

Figure 4. Absorption performance of RhB dye on the surface of filter network device (a) without and (b) with SE-TENG. The photographs were taken (a1, b1) at 5 min, (a2, b2) at 10 min, and (a3, b3) at 15 min. (c) The visible region absorption spectra shows the changing dosage of absorbed RhB on the surface of filter network; left spectra and right spectra were recorded without and with SE-TENG, respectively. (d) The absorption intensity recorded at the characteristic wavelength of RhB (554 nm).

S3. Hence, the energy generation process can be achieved. In this filter system, the SE-TENG was used as the source of electrostatic field, and the output performance of the device was systematically illustrated in Figure 3a,b. The detailed structure of the SE-TENG device can be seen in the inset of Figure 3a. The dielectric material in the device was the Kapton film with a contacting area of 60 cm^2. The Al foil had the dual function of output electrode and the tribo material for contact with the Kapton film. A linear motor with a working frequency of 1 Hz was applied for driving the SE-TENG, and a continuous electrical signal can be applied on the filter by SE-TENG under the periodic motions. Due to the high output voltage from SE-

DOI: 10.1021/acsnano.7b06451
ACS Nano 2017, 11, 12411−12418

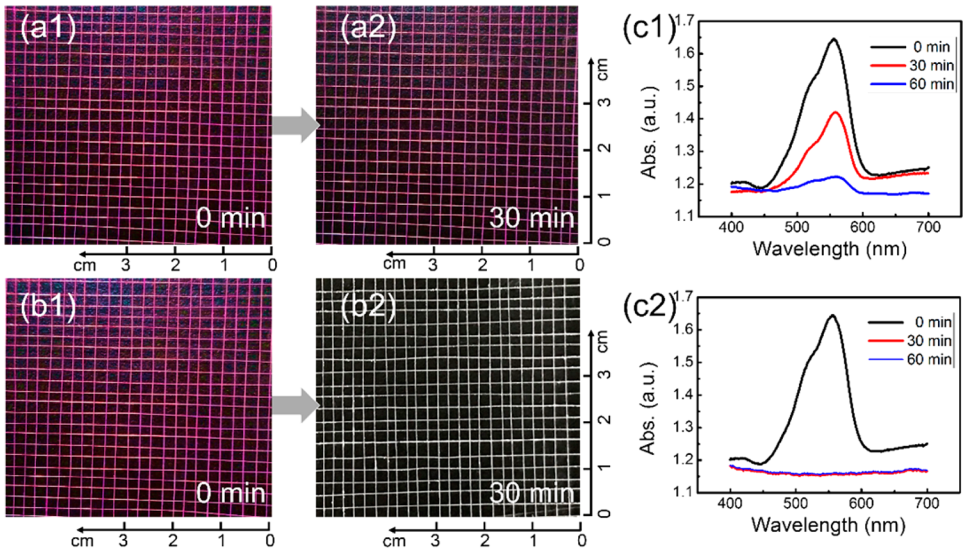

Figure 5. Photocatalytic performance on P25-coated filter network (a) without and (b) with SE-TENG. The filter network irradiated for (a1, b1) 0 min, (a2, b2) 30 min under UV irradiation. The absorption spectrum of the filter network surface (c1) without and (c2) with SE-TENG.

TENG, we modified an electrometer (Trek Model 344) according to our previous work[26] and used the dynamic module to record the performance of SE-TENG. The voltage output applied by SE-TENG is a natural square-wave voltage signal, so no rectifier was used in the process. The open-circuit voltage (V_{oc}) was measured to be about 1900 V in the contact-separation cycles (Figure 3a), showing the high voltage output of SE-TENG. The maximum transferred charges (Q_{sc}) were only 220 nC, and the short-circuit current (I_{oc}) was about 14 μA, as shown in Figure 3b,c. When SE-TENG was connected to the filter network, the established electric field on the filter network was different from the V_{oc} value. As shown in Figure 3c, the maximum voltage on the network was 1110 V under the drive of SE-TENG, indicating that the insulating performance of the filter network was not as good as the open-circuited condition. It was also important to note that the voltage drop of 1110 V on the filter network was enough to realize all the filtering function, and no electrical damage on the filter network had been observed when such a high voltage was applied. The detailed potential distribution on an aperture hole was investigated by using probing technique, as shown in Figure 3e. Since the wires in horizontal direction were contacted to the ground position, the potential signals on the horizontal wires were very weak. In contrast, the detected potentials on the vertical wires (connecting to SE-TENG directly) were exceedingly strong. The highest potentials were located at the points of crossed sites, which were about 700 V relative to ground. Between the nearest two crossed sites, the potentials on the surface showed the sunken distribution along the wire. At the center of the hole, it was only 150 V relative to ground. Meanwhile, the electrostatic field established on the network frame vanished slowly. As shown in Figure 4f, the electrostatic filed induced on the network only decreased 40% after 30 min. It is also important to note that the electrostatic field generated on the network is harmless to human beings, because the Q_{sc} from the SE-TENG is quite small.

RhB aqueous solution was selected as the pollutant sample for the electrostatic filter. After being sprayed out from an atomizer, the tiny RhB droplets can carry some electrostatic charges. With increased spraying time, the red color on the filter surface gradually deepened, and the red area gradually increased. We recorded the photograph of the filter network at 5, 10, and 15 min, respectively, as shown in Figure 4a1−3. It was not obvious in color variation on the filter without the electric field. As explained before, RhB droplets absorbed faster due to Coulomb interactions by applying the strong electrostatic field. Hence, as shown in Figure 4b1−3, the color change of the filter network became very significant under the drive of SE-TENG, which can be quantitatively evaluated using absorption spectra measurement. The visible region absorption spectra of the network at different times are shown in Figure 4c. The absorption intensity at the wavelength of 554 nm for the filter network with and without SE-TENG were recorded, as can be seen in Figure 4d. When combined with a SE-TENG, the absorption intensity of the network surface within 1 min was almost the same intensity achieved within 15 min without SE-TENG, demonstrating a strong electrostatic absorption effect.

The commercial P25 nanoparticles, which can help to degrade the absorbed RhB under UV irradiation, were embedded on the surface of each wire of the filter network (Figure S4). When P25 nanoparticles were embedded on the surface of PTFE-coated stainless steel wires by soaking in a P25/PTFE suspension, those wires exhibited self-cleaning ability after fabrication into mesh network under 60 W UV irradiation, and the color of the filter network was changed due to the degradation. The photographs in Figure 5 a1,a2 were captured after staying in UV light for 0 and 30 min, where the electrostatic field was not applied on the filter. The color changing of the filter was not so significant in Figure 5a1,a2, which indicated a slow degradation process of the RhB. When combined with the SE-TENG, the red dye on the surface faded dramatically. As can be seen in Figure 5b1,b2, RhB was totally deconstructed within 30 min. The visible region absorption spectra of the filter network at different times are shown in Figure 5c, and indicating that the degradation rate was doubled under the drive of SE-TENG.

The fabricated filter network can also be applied to degrade formaldehyde for the indoor air. By loading Pt nanoparticles on commercial P25 in a photoreduction method, the hybrid photocatalyst can possess excellent performance on formaldehyde degradation. UV−Vis diffuse reflectance spectra

DOI: 10.1021/acsnano.7b06451
ACS Nano 2017, 11, 12411−12418

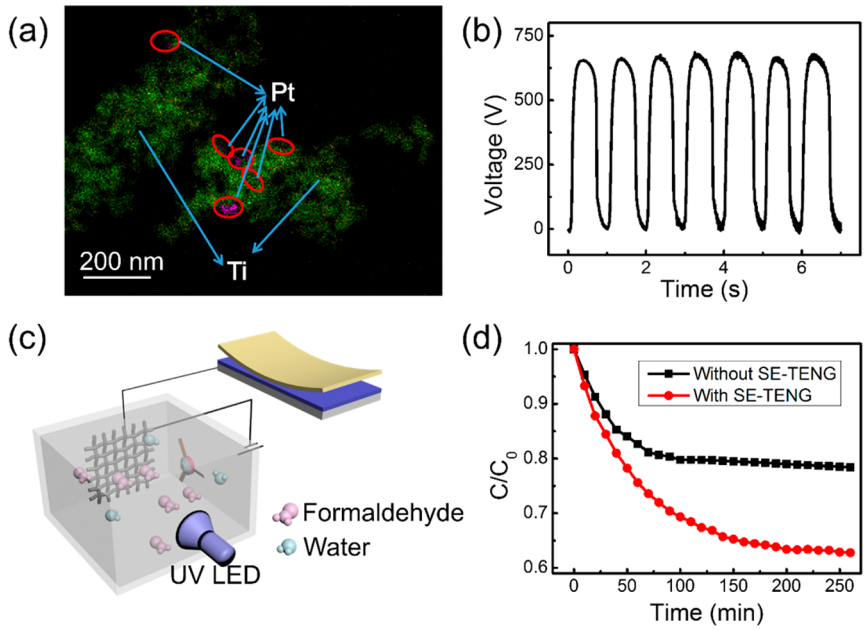

Figure 6. (a) An EDX mapping showing the distribution of Pt and P25 nanoparticles in Pt/P25 powder. The green pixels correspond to Ti element, while red pixels correspond to Pt element. (b) The voltage applied on the Pt/P25-embedded filter network by SE-TENG. (c) The used setup illustration and (d) the concentration change in formaldehyde photocatalytic degradation process with and without SE-TENG.

(DRS) (Figure S5a) showed that Pt/P25 hybrid powder had noticeable absorption in the visible region. However, no obvious corresponding diffraction peaks of metallic Pt were observed (Figure S5b), indicating that the loaded Pt particles were rather small and high dispersed. A high angle annular dark field (HAADF) scanning transmission electron microscope (STEM) image of Pt/P25 is provided in Figure S5c. The large *Z* difference between P25 nanoparticles and Pt metal showed the distribution of Pt nanoparticles. Moreover, the energy dispersive X-ray spectrum (EDX) mapping in Figure 6a showed the distribution of Ti and Pt elements, which also indicated that the distribution of Pt element was successful. After fabrication into the mesh network using the Pt/P25-embedded wires, the voltage on the mesh network dropped to 660 V, as shown in Figure 6b, which was possibly due to the increasing conductivity of the PTFE/parylene layer resulting from the embedding of Pt nanoparticles.

To evaluate the photocatalytic degradation of gaseous formaldehyde, Pt/P25 alcohol dispersion was dip-coated on a piece of glass (100 cm^2). The total photocatalyst on glass was quantified to be 5 mg. An absorption−desorption equilibrium on photocatalyst was established before the photocatalytic degradation of formaldehyde by circulating convection for 60 min. Under UV irradiation (365 nm LED, 80 W), the concentration of formaldehyde decreased dramatically as a function of time, and formaldehyde was totally degraded after 210 min, which demonstrated excellent formaldehyde removal ability of Pt/P25 photocatalyst (see Figure S5d).

As discussed, application of SE-TENG on the polymer-coated network could enhance the adsorption ability of charged droplets and microparticles by the Coulomb force. Since the formaldehyde molecule is polar, the absorption equilibrium state on the surface of the network was re-established under the force of the electrostatic field when the filter was connected to SE-TENG. Accordingly, the absorption of formaldehyde molecules was enhanced as was the case for RhB molecules. Similarly, in some previous reports, the polarized surface could increase the adsorption of polar ions and gaseous molecules, such as Ag^+, RhB in solution, and gaseous ethanol.[29−31] In this case, the formaldemeter was ineffective to detect the dosage of increased gaseous formaldehyde absorbed on the filter network due to the sensitivity and unmatched absorption dosage to total formaldehyde. Under UV irradiation, formaldehyde molecules degrade due to photocatalytic effect. Meanwhile, the photocatalytic performance was enhanced by the electrostatic field from SE-TENG, which was similar to the case of RhB degradation. As shown in Figure 6d, under the drive of the SE-TENG, the formaldehyde concentration decreased to 60% within 250 min, while the formaldehyde concentration only decreased to 80% without SE-TENG. This result suggested that the degradation efficiency was doubled compared with the case without SE-TENG, showing the synergistic effect of electrostatic field enhanced absorption and TENG-enhanced photocatalytic degradation. More experiments were performed to confirm the enhanced photocatalytic property of this TENG-built-in filter. SE-TENGs with different working frequencies (0.5, 1, 2 Hz) as the sources of electrostatic field were selected to show the relation between the degradation effect and the SE-TENG working frequency. The results in Figure S6c indicated that the formaldehyde degradation rate increased with the SE-TENG working frequency. Furthermore, it suggested that it can realize further degradation on more filters (Figure S6d). Compared with a DC power supply (500 V), the formaldehyde degradation rate on the filter (Figure S7) was still 5% higher when combined with a SE-TENG at the working frequency of 1 Hz. The above results proved the concept of this self-powered filtering method based on TENG technique. Prospectively, the integrated filter and SE-TENG, as shown in Figure S8, can be potentially applied in daily life.

Furthermore, a shouter window device was also fabricated to show the triboelectric-enhanced photocatalytic degradation method as shown in Figure S9. In order to avoid short-circuit, a designed insulative slice was used to separate the neighboring louvered battens. The louvered battens were made of Al foil

DOI: 10.1021/acsnano.7b06451
ACS Nano 2017, 11, 12411−12418

and were prepared by the same method as that in Pt/P25/PTFE/parylene-coated stainless steel wire preparation. The result of formaldehyde photocatalytic degradation on shouter device with SE-TENG was also higher than that without SE-TENG, which proved the universal strategy of triboelectric-enhanced adsorption and enhanced photocatalytic degradation method.

CONCLUSIONS

In summary, we demonstrated a concept of self-powered filtering method based on TENG technique for purifying the indoor atmosphere. The photocatalyst P25 or Pt/P25 for degrading the pollutants was embedded on the surface of polymer-coated stainless steel wires, and then the steel wires were woven into a filtering network. A SE-TENG with a contact area of 60 cm^2 was connected to the filtering network, where contact-separation motion could generate a strong electric field over 1100 V on the filter network. In order to demonstrate the electrostatic absorption capability of the device, RhB steam was selected as the pollutant. The absorbed RhB on the local filter network within 1 min under the drive of TENG was almost the same amount of absorption achieved within 15 min without TENG. The high electrostatic field from TENG can also enhance the photocatalytic degradation of RhB, where the time for the degradation of RhB was decreased more than 50% with the help of TENG. Hence, both electrostatic adsorption and TENG-enhanced photocatalytic effect can be achieved on this filter device. Finally, the same network was employed for the degradation of formaldehyde, where degradation efficiency within the same time was doubled under the drive of SE-TENG. This work is a combinational study of TENG technique and photocatalytic air-pollution degradation, which can broaden the applications of self-powered nanosystems. The demonstrated concept can be widely used in the field of haze governance, indoor air cleaning, and photocatalytic pollution removal.

EXPERIMENTAL SECTION

Fabrication of the SE-TENG. The SE-TENG was fabricated according to the previous work.[26] A thin Al foil was adhered to an acrylic board and was used as an electrode. A thin kapton film was fixed on a linear motor and was used as the friction layer.

Preparation of Pt/P25 Photocatalyst. The Pt/P25 photocatalyst was prepared by a photoreduction process. P25 powder (1.0 g, Degussa) was first dispersed in mixture solution of 150 mL of DI water and 50 mL of alcohol. Then, H_2PtCl_6 solution was added dropwise into the previous solution. The formed suspension was stirred for 30 min. After that, a 365 nm LED (CEAULIGHT, 100 W) was vertically irradiated upon the mixture for 1 h. As a result, the gray powder was collected with water and ethanol wash, followed by drying process. The loading of Pt nanoparticles was estimated to be about 1 wt %.

Fabrication of the Filter Network. First, the stainless steel wires (φ = 100 μm) were thoroughly washed in the ethanol and DI water. After the drying process, the wires were coated with a 3 μm parylene layer through chemical vapor deposition (LACHI, LH300). The coated wires were then soaked in a polytetrafluoroethylene (PTFE) solution (DuPont, 60 wt %) followed by P25/PTFE or Pt/P25/PTFE dispersion (P25 0.5 wt %). After annealing at 300 °C for 10 min, the wires were woven into a mesh structure in an acrylic frame. To stabilize the wires and ensure electric conductivity, the contact sections were sealed with Al tape, which served as current collector.

Characterization of the Device. The output characteristics, including voltage output, current output, transferred charges, and potential distribution, were recorded by Trek model 344 electrometer and Keithley 6514 system electrometer. The morphology of photocatalyst and polymer-coated wires were characterized with a scanning electron microscope (SEM, HITACHI S4800) and a field emission transmission electron microscope (FETEM, FEI Tecnai G2 F20 S-TWIN). The crystal structures of photocatalysts were analyzed by an X-ray diffractometer (XRD, Panalytical Xpert 3 powder, Cu Kα radiation). UV−vis diffuse reflectance spectra (DRS) were obtained by using a spectrophotometer (Shimadzu UV 3600) with an integrating sphere attachment and with $BaSO_4$ as reflectance standard.

Adsorption of RhB Dye. The adsorption of RhB on the filter network was carried out by a homemade setup. The RhB solution (500 ppm) was sprayed out at the spray flux of 0.2 mL/min by an air compressor atomizer (nozzle diameter = 17 mm, barometric pressure = 0.2 MPa), and the filter network was placed vertically 10 cm away from the nozzle. After certain spraying time, the surface color and absorption spectrum were characterized by digital photos and spectrophotometer (Shimadzu UV 3600).

Photocatalytic Degradation of RhB Dye. To carry out the photocatalytic degradation of RhB on the filter network, the fabricated device was first immersed in RhB solution (500 ppm) for 5 min to establish the absorption equilibrium. For the test, the device was placed under the irradiation of a 365 nm LED (CEAULIGHT, 60 W). Such discoloration process was recorded by digital pictures and spectrophotometer (Shimadzu UV 3600).

Photocatalytic Degradation of Formaldehyde. The photocatalytic degradation of formaldehyde was carried out in a quartz box (27 L). Before the quartz box was sealed, 5 μL of diluted formaldehyde solution was injected into the box, and a tiny fan was used to circulate the sealed air. The concentration of formaldehyde was measured to be 1.0 ± 0.05 ppm at the equilibrium stage. A 365 nm LED (CEAULIGHT, 80 W) was irradiated vertically upon the fabricated filter network with a distance of 10 cm to carry out the photocatalytic degradation process. The concentration of formaldehyde in the quartz box was recorded by a formaldemeter (PPM Tech. Ltd. HTV-m).

ASSOCIATED CONTENT

Supporting Information

The Supporting Information is available free of charge on the ACS Publications website at DOI: 10.1021/acsnano.7b06451.

SEM images of noncoated and coated stainless steel, photograph of the fabricated network device with P25/PTFE/parylene-coated wires and the general fabrication diagram of the network device, the working principle of SE-TENG in cycles, photocurrent output on P25 photoelectrode and photocatalytic degradation of RhB dye performance on P25 nanoparticles, DRS, XRD, and STEM pattern of Pt/P25, the photocatalytic performance of formaldehyde degradation on the filter, the performance with different power supply, the proposed filter usage in the daily life and the components of the filter, the fabricating illustration and digital photographs of the shutter device, the voltage on the device and the photocatalytic performance of formaldehyde degradation with and without SE-TENG (PDF)

AUTHOR INFORMATION

Corresponding Authors

*E-mail: chenxiangyu@binn.cas.cn.
*E-mail: bianzhenfeng@shnu.edu.cn.
*E-mail: hexing-li@shnu.edu.cn.
*E-mail: zlwang@gatech.edu.

ORCID

Zhenfeng Bian: 0000-0001-7552-8027
Zhong Lin Wang: 0000-0002-5530-0380

Notes

The authors declare no competing financial interest.

DOI: 10.1021/acsnano.7b06451
ACS Nano 2017, 11, 12411−12418

ACKNOWLEDGMENTS

This work is supported by National Natural Science Foundation of China (Grant No. 21237003, 21407106, 21522703, 21377088, 51432005, 5151101243, 51561145021, and 51775049), Shanghai Government (Grants 14ZR1430800, 13SG44 and 15520711300), International Joint Laboratory on Resource Chemistry (IJLRC), the National Key R & D Project from Minister of Science and Technology (Grant 2016YFA0202704), and Beijing Municipal Science & Technology Commission (Grant Y3993113DF). Research is also supported by The Program for Professor of Special Appointment (Eastern Scholar) at Shanghai Institutions of Higher Learning and the Ministry of Education of China (Grant PCSIRT_IRT_16R49).

REFERENCES

(1) Zhang, R. Atmospheric Science: Warming Boosts Air Pollution. *Nat. Clim. Change* **2017**, *7*, 238−239.
(2) Anenberg, S. C.; Miller, J.; Minjares, R.; Du, L.; Henze, D. K.; Lacey, F.; Malley, C. S.; Emberson, L.; Franco, V.; Klimont, Z.; Heyes, C. Impacts and Mitigation of Excess Diesel-Related NO_x Emissions in 11 Major Vehicle Markets. *Nature* **2017**, *545*, 467−471.
(3) Nel, A. Air Pollution-Related Illness: Effects of Particles. *Science* **2005**, *308*, 804−806.
(4) Mølhave, L. Volatile Organic Compounds, Indoor Air Quality and Health. *Indoor Air* **1991**, *1*, 357−376.
(5) Liu, C.; Hsu, P. C.; Lee, H. W.; Ye, M.; Zheng, G. Y.; Liu, N. A.; Li, W. Y.; Cui, Y. Transparent Air Filter for High-Efficiency PM2.5 Capture. *Nat. Commun.* **2015**, *6*, 6205.
(6) Lee, K. J.; Shiratori, N.; Lee, G. H.; Miyawaki, J.; Mochida, I.; Yoon, S.-H.; Jang, J. Activated Carbon Nanofiber Produced from Electrospun Polyacrylonitrile Nanofiber as a Highly Efficient Formaldehyde Adsorbent. *Carbon* **2010**, *48*, 4248−4255.
(7) Aydogan, A.; Montoya, L. D. Formaldehyde Removal by Common Indoor Plant Species and Various Growing Media. *Atmos. Environ.* **2011**, *45*, 2675−2682.
(8) Fisher, G. L.; Chang, D. P. Y.; Brummer, M. Fly Ash Collected from Electrostatic Precipitators: Microcrystalline Structures and the Mystery of the Spheres. *Science* **1976**, *192*, 553−555.
(9) Fan, F.-R.; Lin, L.; Zhu, G.; Wu, W.; Zhang, R.; Wang, Z. L. Transparent Triboelectric Nanogenerators and Self-Powered Pressure Sensors Based on Micropatterned Plastic Films. *Nano Lett.* **2012**, *12*, 3109−3114.
(10) Fan, F.-R.; Tian, Z.-Q.; Wang, Z. L. Flexible Triboelectric Generator. *Nano Energy* **2012**, *1*, 328−334.
(11) Wang, Z. L.; Jiang, T.; Xu, L. Toward the Blue Energy Dream by Triboelectric Nanogenerator Networks. *Nano Energy* **2017**, *39*, 9−23.
(12) Wang, Z. L. Triboelectric Nanogenerators as New Energy Technology for Self-Powered Systems and as Active Mechanical and Chemical Sensors. *ACS Nano* **2013**, *7*, 9533−9557.
(13) Zhang, X.-S.; Han, M.-D.; Wang, R.-X.; Meng, B.; Zhu, F.-Y.; Sun, X.-M.; Hu, W.; Wang, W.; Li, Z.-H.; Zhang, H.-X. High-Performance Triboelectric Nanogenerator with Enhanced Energy Density Based on Single-Step Fluorocarbon Plasma Treatment. *Nano Energy* **2014**, *4*, 123−131.
(14) Jiang, T.; Zhang, L. M.; Chen, X.; Han, C. B.; Tang, W.; Zhang, C.; Xu, L.; Wang, Z. L. Structural Optimization of Triboelectric Nanogenerator for Harvesting Water Wave Energy. *ACS Nano* **2015**, *9*, 12562−12572.
(15) Pu, X.; Li, L.; Song, H.; Du, C.; Zhao, Z.; Jiang, C.; Cao, G.; Hu, W.; Wang, Z. L. A Self-Charging Power Unit by Integration of a Textile Triboelectric Nanogenerator and a Flexible Lithium-Ion Battery for Wearable Electronics. *Adv. Mater.* **2015**, *27*, 2472−2478.
(16) Xi, Y.; Wang, J.; Zi, Y.; Li, X.; Han, C.; Cao, X.; Hu, C.; Wang, Z. High Efficient Harvesting of Underwater Ultrasonic Wave Energy by Triboelectric Nanogenerator. *Nano Energy* **2017**, *38*, 101−108.
(17) Chen, X.; Pu, X.; Jiang, T.; Yu, A.; Xu, L.; Wang, Z. L. Tunable Optical Modulator by Coupling a Triboelectric Nanogenerator and a Dielectric Elastomer. *Adv. Funct. Mater.* **2017**, *27*, 1603788.
(18) Chen, X.; Wu, Y.; Yu, A.; Xu, L.; Zheng, L.; Liu, Y.; Li, H.; Wang, Z. L. Self-Powered Modulation of Elastomeric Optical Grating by Using Triboelectric Nanogenerator. *Nano Energy* **2017**, *38*, 91−100.
(19) Cui, N.; Gu, L.; Liu, J.; Bai, S.; Qiu, J.; Fu, J.; Kou, X.; Liu, H.; Qin, Y.; Wang, Z. L. High Performance Sound Driven Triboelectric Nanogenerator for Harvesting Noise Energy. *Nano Energy* **2015**, *15*, 321−328.
(20) Gu, G. Q.; Han, C. B.; Lu, C. X.; He, C.; Jiang, T.; Gao, Z. L.; Li, C. J.; Wang, Z. L. Triboelectric Nanogenerator Enhanced Nanofiber Air Filters for Efficient Particulate Matter Removal. *ACS Nano* **2017**, *11*, 6211−6217.
(21) Han, C. B.; Jiang, T.; Zhang, C.; Li, X.; Zhang, C.; Cao, X.; Wang, Z. L. Removal of Particulate Matter Emissions from a Vehicle Using a Self-Powered Triboelectric Filter. *ACS Nano* **2015**, *9*, 12552−12561.
(22) Chen, S.; Gao, C.; Tang, W.; Zhu, H.; Han, Y.; Jiang, Q.; Li, T.; Cao, X.; Wang, Z. Self-Powered Cleaning of Air Pollution by Wind Driven Triboelectric Nanogenerator. *Nano Energy* **2015**, *14*, 217−225.
(23) Tang, C.; Liu, L.; Li, Y.; Bian, Z. Aerosol Spray Assisted Assembly of TiO_2 Mesocrystals into Hierarchical Hollow Microspheres with Enhanced Photocatalytic Performance. *Appl. Catal., B* **2017**, *201*, 41−47.
(24) Zhu, W.; Xiao, S.; Zhang, D.; Liu, P.; Zhou, H.; Dai, W.; Liu, F.; Li, H. Highly Efficient and Stable Au/CeO_2−TiO_2 Photocatalyst for Nitric Oxide Abatement: Potential Application in Flue Gas Treatment. *Langmuir* **2015**, *31*, 10822−10830.
(25) Liu, J.; Zhang, C.; Ma, B.; Yang, T.; Gu, X.; Wang, X.; Zhang, J.; Hu, C. Rational Design of Photoelectron-Trapped/Accumulated Site and Transportation Path for Superior Photocatalyst. *Nano Energy* **2017**, *38*, 271−280.
(26) Zheng, L.; Wu, Y. L.; Chen, X. Y.; Yu, A. F.; Xu, L.; Liu, Y. S.; Li, H. X.; Wang, Z. L. Self-Powered Electrostatic Actuation Systems for Manipulating the Movement of both Microfluid and Solid Objects by Using Triboelectric Nanogenerator. *Adv. Funct. Mater.* **2017**, *27*, 1606408.
(27) Choi, D.; Lee, H.; Im, D. J.; Kang, I. S.; Lim, G.; Kim, D. S.; Kang, K. H. Spontaneous Electrical Charging of Droplets by Conventional Pipetting. *Sci. Rep.* **2013**, *3*, 2037.
(28) Zheng, L.; Lin, Z.-H.; Cheng, G.; Wu, W.; Wen, X.; Lee, S.; Wang, Z. L. Silicon-Based Hybrid Cell for Harvesting Solar Energy and Raindrop Electrostatic Energy. *Nano Energy* **2014**, *9*, 291−300.
(29) Cui, Y.; Briscoe, J.; Dunn, S. Effect of Ferroelectricity on Solar-Light-Driven Photocatalytic Activity of $BaTiO_3$−Influence on the Carrier Separation and Stern Layer Formation. *Chem. Mater.* **2013**, *25*, 4215−4223.
(30) Jones, P. M.; Dunn, S. Interaction of Stern Layer and Domain Structure on Photochemistry of Lead-Zirconate-Titanate. *J. Phys. D: Appl. Phys.* **2009**, *42*, 065408.
(31) Zhao, M. H.; Bonnell, D. A.; Vohs, J. M. Effect of Ferroelectric Polarization on the Adsorption and Reaction of Ethanol on $BaTiO_3$. *Surf. Sci.* **2008**, *602*, 2849−2855.

DOI: 10.1021/acsnano.7b06451
ACS Nano 2017, 11, 12411−12418